A ‘frozen electric-field’ approach to simulate repetitively pulsed nanosecond plasma discharges and ignition of hydrogen–air mixtures

2014 J. Phys. D: Appl. Phys. 47 385201

(http://iopscience.iop.org/0022-3727/47/38/385201)

IOP Publishing Journal of Physics D: Applied Physics
J. Phys. D: Appl. Phys. **47** (2014) 385201 (11pp) doi:10.1088/0022-3727/47/38/385201

A 'frozen electric-field' approach to simulate repetitively pulsed nanosecond plasma discharges and ignition of hydrogen–air mixtures

Sharath Nagaraja and Vigor Yang

School of Aerospace Engineering Georgia Institute of Technology, Atlanta, GA 30332-0150, USA

E-mail: vigor@gatech.edu

Received 27 April 2014, revised 21 July 2014
Accepted for publication 4 August 2014
Published 28 August 2014

Abstract

High-fidelity modelling of nanosecond repetitively pulsed discharges (NRPDs) is burdened by the multiple time and length scales and large chemistry mechanisms involved, which prohibit detailed analyses and parametric studies. In the present work, we propose a 'frozen electric-field' modelling approach to expedite the NRPD simulations without adverse effects on the solution accuracy. First, a burst of nanosecond voltage pulses is simulated self-consistently until the discharge reaches a stationary state. The calculated spatial distributions and temporal evolution of the electric field, electron density and electron energy during the last pulse are then stored in a library and the electrical characteristics of subsequent pulses are frozen at these values. This strategy allows the timestep for numerical integration to be increased by four orders of magnitude (from 10^{-13} to 10^{-9} s), thereby significantly improving the computational efficiency of the process. Reduced calculations of a burst of 50 discharge pulses show good agreement with the predictions from a complete plasma model (electrical characteristics calculated during each pulse). The error in species densities is less than 20% at the centre of the discharge volume and about 30% near the boundaries. The deviations in temperature, however, are much lower, at 5% in the entire domain. The model predictions are in excellent agreement with measured ignition delay times and temperatures in H_2–air mixtures subject to dielectric barrier NRPD over a pressure range of 54–144 Torr with equivalence ratios of 0.7–1.2. The OH density increases with pressure and triggers low-temperature fuel oxidation, which leads to rapid temperature rise and ignition. The ignition delay decreases by a factor of 2, with an increase in pressure from 54 to 144 Torr. In contrast, an increase in the H_2–air equivalence ratio from 0.7 to 1.2 marginally decreases the ignition delay by about 20%. This behaviour is attributed to the insensitivity of OH production rates to the variation in the equivalence ratio.

Keywords: modelling of nanosecond discharges, plasma assisted combustion, plasma physics

(Some figures may appear in colour only in the online journal)

1. Introduction

In recent years, there has been significant interest in utilizing nanosecond repetitively pulsed discharges (NRPDs) for combustion enhancement [1–4], flow control [5–7], and biomedical applications [8–11]. In these discharges, the reduced electric field (E/N, ratio of the electric field magnitude to the number density) is in the range of 100–1000 Td ($1\,\mathrm{Td} = 10^{-17}\,\mathrm{V\,cm^2}$) [1]. As a consequence, a large fraction of input energy is consumed in electron impact molecular dissociation and excitation of internal energy, generating a variety of active species and gas heating.

High-fidelity NRPD simulations can be immensely beneficial in understanding the complex electric-field dynamics and in quantifying the key kinetic pathways for active species production and their ensuing chemical reactions. There have been significant efforts in developing self-consistent models of nanosecond discharges for various applications [5, 6, 11–14]. In this context, self-consistency refers to the numerical solution of the coupled system of equations for the electric potential, charged and neutral species continuity and flow dynamics, without any adjustable parameters. Unfer *et al* [5] proposed a 2D model to study the interaction of the flow over a flat plate with a surface barrier nanosecond discharge in air, for plasma flow control. The chemical kinetics scheme was composed of only two species, to reduce the computational burden. Fast gas heating and formation of compression waves were investigated using a phenomenological model for thermalization. Poggie *et al* [6] carried out 1D simulations of nanosecond dielectric barrier discharges in air with a detailed chemical kinetics scheme consisting of 23 species and 50 reactions. The model was able to predict the generation of weak compression waves through fast gas heating from quenching of excited species. Breden *et al* [11] performed 2D simulations of nanosecond streamer plasma propagation in a helium jet ejecting into quiescent air, a topic of interest in biomedical applications. Detailed chemical kinetics (16 species and 40 reactions) and photoionization effects were taken into account to provide fundamental insight into the streamer dynamics. It must be emphasized that high computational costs restricted these analyses [5, 6, 11] to simulate a single nanosecond voltage pulse.

Recently, one-dimensional, self-consistent simulations of multiple (more than 100) nanosecond discharge pulses were conducted for air [12] and H_2–air mixtures [13], with detailed chemical kinetics at low pressures (40–160 Torr). An adaptive timestep approach was utilized to tackle the large disparity in time scales of various physical phenomena. An efficient technique was proposed [13] to systematically reduce nonequilibrium plasma chemistry mechanisms. The pulsed discharge simulations of H_2–air mixtures using the optimized chemistry mechanism were three times faster than the corresponding calculations performed with a detailed kinetics dataset.

The multi-scale nature of pulsed nanosecond discharges [12] creates enormous numerical challenges. Numerical timesteps of the order of 10^{-13} s are needed to resolve the electric-field transients during each voltage pulse. On the other hand, cumulative kinetic and thermal effects of multiple discharge pulses (ms timescales) are of practical interest. In addition, these nonequilibrium discharges produce a variety of chemical species and excited states. The severe numerical stiffness introduced by large chemistry mechanisms necessitates the use of expensive implicit or semi-implicit solution techniques. It is practically impossible to perform broad parametric studies or multi-dimensional simulations with detailed chemical kinetics using numerical timesteps of the order of 10^{-13} s during each voltage pulse. Judicious simplifications in the numerical framework are required to expedite the calculations without compromise of the accuracy of results.

During a nanosecond voltage pulse, the production rate of electrons is a function of the gas number density, mixture composition and initial electron concentration (residual or remnant charges from the previous pulse) in the discharge gap. The residual electron density is dependent on the ion–electron recombination and electron attachment rates which are sensitive to the pressure and mixture composition, respectively. In addition, the flow residence time and pulsing frequency affects the residual charge concentrations. The flowfield has negligible impact on the discharge dynamics, so long as $U_f \times T_i \ll d_g$, where U_f is the flow velocity, T_i the time interval between two consecutive pulses, and d_g the gap between the electrodes. The plasma generated radicals and excited species have a weak impact on the discharge development, due to their low concentrations (typically less than 1%). Consequently, the electrical dynamics during a burst of nanosecond discharge pulses may exhibit periodic behaviours for low flow velocities and in the absence of significant variations in the gas number density or mixture composition. Tholin *et al* [14] observed similar behaviour in their 2D simulations of pulsed nanosecond discharges in a pin–pin geometry at 1 atm pressure. The plasma reached a 'quasi-periodic' glow regime with repetitive application of voltage waveforms. The spatio-temporal evolution of the electric field and electron density remained constant during each pulse.

The objectives of this work are twofold. First, we propose a 'frozen electric-field' modelling approach to expedite the NRPD simulations without adverse effects on the correctness of solutions. The procedure involves two steps. A burst of nanosecond voltage pulses is simulated using the self-consistent, nonequilibrium plasma modelling framework described in [12, 13]. The simulation is continued until the discharge reaches a stationary state, i.e. the electrical characteristics during two consecutive voltage pulses show variations within a specified bound. The calculated spatial distributions and temporal evolution of the electric field, electron density and electron energy are then stored in a library. Next, the calculations of these properties are suspended. The electrical characteristics of subsequent pulses are frozen at the values in the library. By adopting this strategy, the timestep for numerical integration can be increased by four orders of magnitude (from 10^{-13} to 10^{-9} s), thereby significantly improving the computational efficiency. Second, we make use of the 'frozen electric-field' modelling approach to conduct a detailed parametric study to understand the effect of pressure (54–144 Torr) and equivalence ratio (0.7–1.2) on H_2–air ignition properties subject to pulsed nanosecond discharges.

Starikovskii *et al* [15] used ICCD imaging to show that plane-to-plane pulsed nanosecond dielectric barrier discharges in air at 300 K are filamentary and nonuniform even at low pressures (10–100 Torr). Kinetic analysis revealed that the inhomogeneity in plasma energy addition significantly affected the ignition properties of fuel–air mixtures. Yin *et al* [16], on the other hand, demonstrated that preheating (400–500 K) can significantly improve plasma uniformity in H_2–air mixtures. ICCD images illustrated that the plasma remain uniform and

devoid of any filaments at these conditions. In the present work, we conduct one-dimensional simulations of pulsed nanosecond dielectric barrier discharges in a plane-to-plane geometry at low pressures in H_2–air mixtures with detailed chemical kinetics to validate the frozen electric-field modelling approach. The 1D assumption is justified by the uniform and diffuse plasma observed by Yin *et al* [16] in an identical configuration under similar operating conditions.

The paper is organized as follows. Section 2 describes the simulation configuration and the modelling framework. In section 3.1, a burst of 10 ns voltage pulses is simulated using a complete plasma model with electrical characteristics calculated during each pulse, in order to demonstrate the periodic nature of NRPD. The frozen electric-field modelling approach is then described in section 3.2, and its predictions are benchmarked against those of the complete plasma model. In section 3.3, ignition of H_2–air mixtures subject to dielectric barrier NRPD is simulated using the frozen approach over a range of pressures (54–144 Torr) and equivalence ratios (0.7–1.2). The calculated ignition delay and temperature are compared with experimental measurements reported in [17] to critically assess the accuracy and robustness of the frozen modelling strategy.

2. Theoretical framework

2.1. Physical configuration

Figure 1(*a*) shows schematically the physical configuration of concern, simulating the plasma flow reactor experiment described in [17]. The quartz walls are 1.75 mm thick, and separated from each electrode by a 1.58 mm thick high temperature dielectric adhesive sheet (silicone rubber). The discharge gap is 1 cm wide and is filled with a mixture of H_2 and dry air (79% N_2, 21% O_2). The dielectric constant for quartz is $\varepsilon_g = 3.8$. The dielectric constant of silicone rubber is strongly dependent on its chemical composition and temperature ($\varepsilon_s = 3.2$–9.8) [17]. This introduces significant uncertainty in the coupled energy during nanosecond voltage pulses [13]. We performed a sensitivity study and found that $\varepsilon_s = 6.0$ provided the best match between the calculated and measured ignition delay times. In all the simulations presented in this work, the dielectric constant of silicone rubber is fixed at 6.0. The right electrode is connected to a high voltage power supply (CPT pulser), whereas the left electrode is grounded. Figure 1(*b*) shows the measured nanosecond waveforms, along with the curve-fits used in the present simulations. The CPT waveform consists of a bipolar pulse of duration 100 ns, with peak voltages of −22.5 kV and 17.5 kV in the negative and positive half cycles, respectively. The simulations are conducted with pressures in the range of 54–144 Torr, equivalence ratios between 0.7–1.2, and pulsing frequencies between 20–40 kHz.

2.2. Governing equations

The self-consistent NRPD model employed in the present work is described in detail in [12, 13]. Conservation equations for the electric potential, electron energy, and charged and neutral species are considered. The formulation also accommodates conservation of mass, momentum and energy of the gas mixture to characterize flow motions. The electron transport and reaction coefficients are expressed as functions of electron energy using the BOLSIG software [18]. Details about the numerical methods and associated initial and boundary conditions can be found in [12].

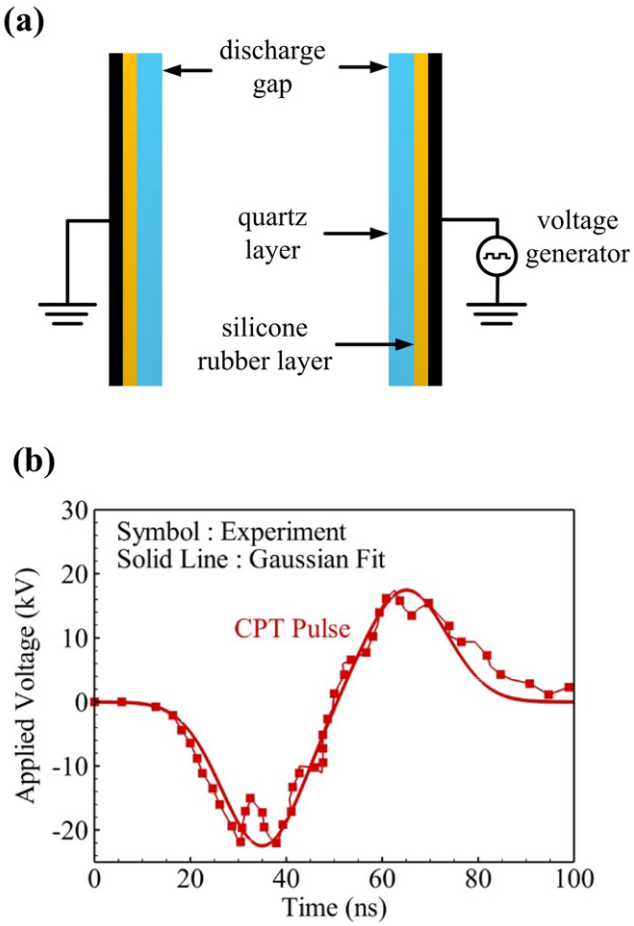

Figure 1. (*a*) Schematic of simulation configuration. (*b*) CPT experimental waveform and corresponding curve-fit used in model calculations.

In the frozen approach, the electric-field dynamics are calculated for a few voltage pulses until the discharge reaches a stationary state. The electrical characteristics in subsequent pulses then remain fixed, with calculations of the electric potential, electron density, and electron energy suspended until the end of the simulation.

2.3. Initial and boundary conditions

At solid walls, a zero-flux boundary condition is imposed for the conservation equations of mass and momentum and neutral species concentrations. Ion and electron fluxes at the boundaries are expressed as the sum of the drift (due to electric field) and thermal velocity components. The electron flux also includes a secondary emission component at the cathode. Boundary conditions for the gas energy equation must be properly specified to predict the temperature evolution in the

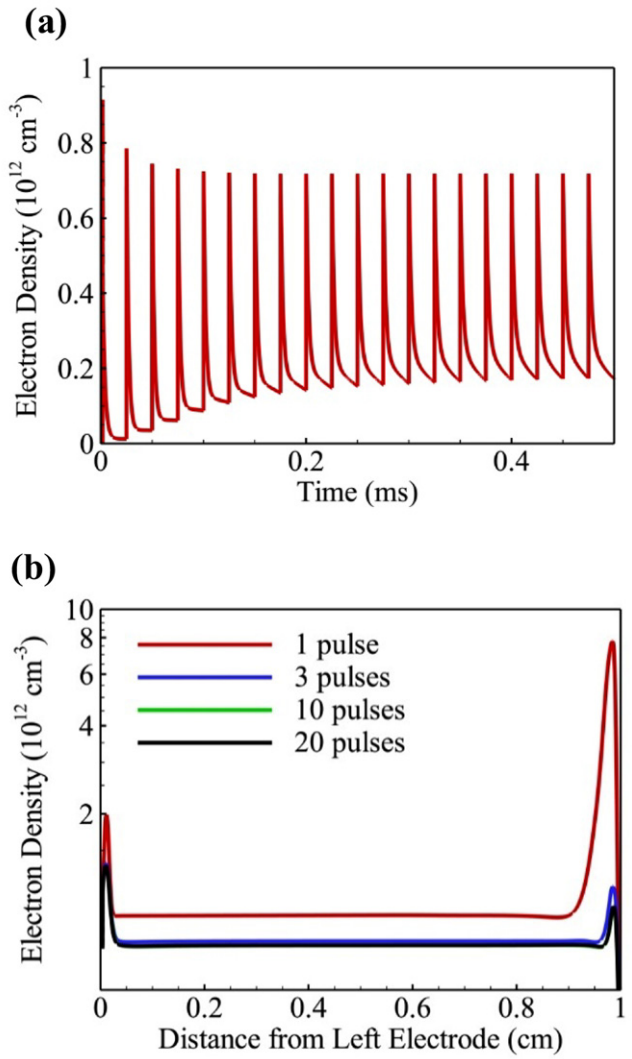

Figure 2. (*a*) Temporal evolution of electron density versus time at the centre of the discharge domain. (*b*) Spatial distribution of electron density immediately after 1st, 3rd, 10th and 20th pulses ($P_i = 114$ Torr, $T_i = 473$ K, $\phi = 1$, $f = 40$ kHz).

discharge volume. In this work, we make use of the wall boundary conditions derived in [12] by treating the dielectric layer as a semi-infinite solid. The initial $H_2/O_2/N_2$ densities are determined based on the initial pressure, temperature and equivalence ratio. The remaining species densities are initialized to 10^8 cm^{-3}, except for electron density, which is initially set at 2×10^8 cm^{-3} to ensure charge neutrality.

2.4. Numerical methods

The conservation equations are solved by means of a second-order Strang splitting method to treat convection–diffusion and chemical source terms separately [12]. Implicit time integration is performed for stiff chemical source terms, whereas species and flow transport is solved explicitly for improved computational efficiency. A domain decomposition approach with MPI (message passing interface) is implemented to facilitate parallel computation over 48 processors. In all the simulations, a non-uniform mesh with 600 nodes is used to obtain grid independent solutions [13]. For the complete plasma model, we use adaptive time-stepping. During each discharge pulse, the timestep is varied between 10^{-13}–10^{-12} s to accurately capture the electric-field transients and the electron energy relaxation process. In the time interval between pulses, the electric field is set to zero and the timestep is fixed at 10^{-9} s. When the electric field is frozen, the timestep is fixed at 10^{-9} s both during and in the time interval between the voltage pulses.

2.5. H_2–air nanosecond plasma ignition kinetics

The baseline H_2–air chemistry mechanism used in the present work has previously been validated [13, 19, 20]. The scheme consists of 19 species and 111 reactions. It incorporates neutral species N_2, H_2, O_2, H, O, O_3, OH, HO_2 and H_2O; charged species N_2^+, HN_2^+, H_3O^+, O_2^- and e^-; and excited species $N_2(A^3)$, $N_2(B^3)$, $N_2(C^3)$, $N_2(a^1)$ and $O(^1D)$. A detailed plasma kinetic analysis [13] showed that dominant positive and negative ions in pulsed nanosecond $H_2/O_2/N_2$ discharges are H_3O^+ and O_2^-, respectively. Atomic oxygen and hydrogen are produced during discharge pulses via electron impact dissociation of O_2 and H_2 molecules, respectively. In the time duration between voltage pulses, quenching of excited N_2 species by O_2 and H_2 also contribute to production of O and H atoms, respectively. At temperatures below 700 K, OH is primarily generated from reactions of HO_2 with O and H radicals.

Takashima *et al* [21] measured N_2 vibrational temperature in air at 60 Torr pressure after a burst of nanosecond plasma pulses in a plane-to-plane geometry. The reported values were quite low, 850 K after 50 pulses and 1050 K after 100 pulses. This behaviour was attributed to the slow rate of plasma energy addition (0.8–1.0 mJ/pulse) and fast vibrational relaxation. In the present work, since the operating conditions are similar to those in [21], vibrational processes are not considered as part of the chemistry mechanism (i.e., instantaneous vibrational relaxation is assumed).

3. Results and discussion

3.1. Periodicity of pulsed nanosecond discharge dynamics

Detailed discussions of the electrical characteristics of NRPD in H_2–air mixtures can be found elsewhere [13]. The focus here is to demonstrate the periodic nature of the discharge dynamics under repetitive application of nanosecond voltage pulses. The self-consistent 1D plasma model described in section 2.2 is used to perform the simulations described in this section. The spatial uniformity of nanosecond plasma at low pressures justifies the 1D assumption [12, 13]. Figure 2(*a*) shows the temporal evolution of electron density at the centre of the discharge volume for a burst of 20 pulses at a pressure of 114 Torr, an initial temperature of 473 K, and a pulsing rate of 40 kHz. It is evident that the electron density reaches a stationary state after 10 pulses. The electron production and decay rates remain the same during each pulse for the remainder of the burst at this location. Figure 2(*b*) shows the spatial distribution of the electron density in the discharge gap

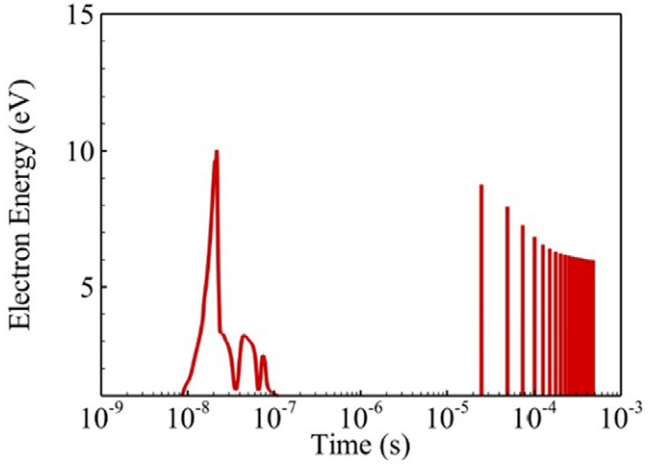

Figure 3. Temporal evolution of electron energy at the centre of the discharge domain ($P_i = 114$ Torr, $T_i = 473$ K, $\phi = 1$, $f = 40$ kHz).

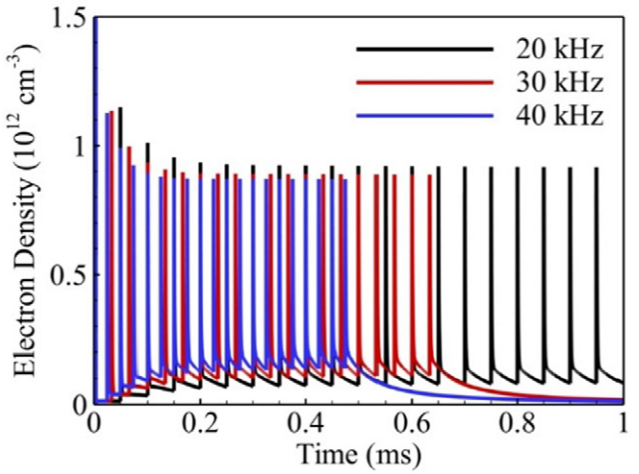

Figure 4. Time evolution of electron density at the centre of the discharge domain for 20 pulses at 20, 30 and 40 kHz repetition rates ($P_i = 114$ Torr, $T_i = 473$ K, $\phi = 1$).

at the end of the 1st, 3rd, 10th and 20th pulses, respectively. The maximum difference in the electron density after the 3rd and 10th pulses is approximately 10%, whereas it is less than 5% between the 10th and 20th pulses. The temporal evolution of the electron energy at the centre of the physical domain is plotted in figure 3, indicating an asymptotic behaviour after 8 pulses, with a peak value of approximately 6.5 eV.

The discharge dynamics at different pulsing frequencies is shown in figure 4. The evolution of the electron density at the centre of the physical domain is for 20 kHz, 30 kHz and 40 kHz, respectively. The initial pressure and temperature are 114 Torr and 473 K, respectively, with the equivalence ratio of $\phi = 1$. In all the three cases, the electron production and decay rates reach a stationary state after a few voltage pulses. It is interesting to note that the peak value of the electron density at steady state decreases with increasing pulse rate from 9×10^{11} cm^{-3} at 20 kHz to 8.5×10^{11} cm^{-3} at 40 kHz, respectively. This behaviour can be attributed to the increase in the residual electron density with increasing repetition rate (i.e., less time is available for electron–ion recombination

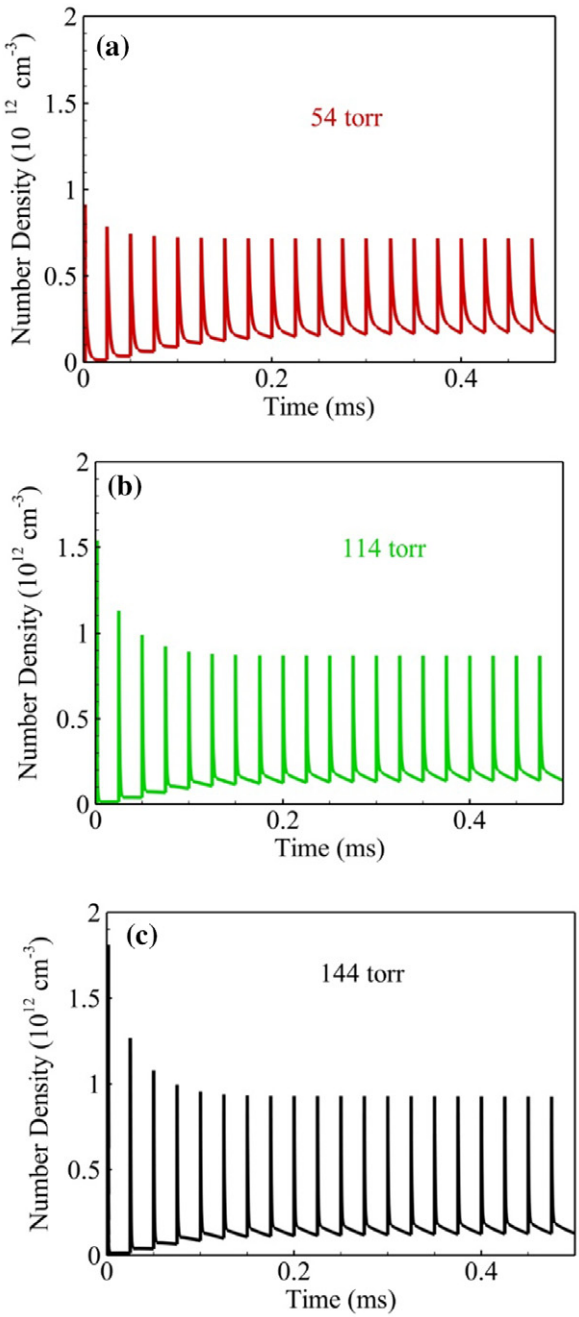

Figure 5. Time evolution of electron density at the centre of the discharge domain for 20 pulses at (*a*) 54 Torr, (*b*) 114 Torr and (*c*) 144 Torr pressures, respectively ($T_i = 473$ K, $\phi = 1$, $f = 40$ kHz).

between pulses). High residual charges result in earlier electrical breakdown during a discharge pulse, consequently leading to reduced ionization rates.

Figure 5 shows the temporal evolution of electron density at the centre of the discharge volume at three different pressures of 54, 114 and 144 Torr. The initial temperature is 473 K and the equivalence ratio is unity. The electron density exhibits periodic behaviour after a few pulses, irrespective of the pressure. The peak electron density at steady state increases with increasing pressure, from 7.5×10^{11} cm^{-3} at 54 Torr to 9.5×10^{11} cm^{-3} at 144 Torr, respectively. Faster recombination rates at high pressures result in lower residual charge densities,

which lead to increase in the ionization rates, and result in higher peak electron density.

In summary, the NRPD, under present operating conditions, reach an asymptotic regime after 10 voltage pulses. The electrical characteristics, such as electron production and decay rates, remain unchanged in subsequent pulses. This behaviour was observed at different pulsing rates and pressures. Although not shown, a similar situation was observed over a range of H_2–air equivalence ratios as well.

The accuracy of the 'frozen electric-field' modelling approach hinges on the criterion used to decide when the pulsed discharge has reached a periodic regime. We found that the maximum difference in the spatial distribution of the electron density at the end of two consecutive voltage pulses ($\Delta n_{e,max}$) provides the best metric. In the present work, we fix $\Delta n_{e,max} \leqslant 5\%$, which is achieved after 10 pulses, and the electrical characteristics are frozen beyond that juncture. The $\Delta n_{e,max}$ criterion is robust and functions well over the range of pressures, pulsing frequencies, and equivalence ratios considered in the present work. Note that a larger cutoff value for $\Delta n_{e,max}$ can be utilized for multi-dimensional pulsed discharge simulations which are more computationally demanding.

3.2. 'Frozen electric-field' modelling approach

In this section, we take advantage of the periodic behaviour shown previously, in order to formulate an efficient strategy to expedite simulations of NRPD. The 'frozen electric-field' approach consist of the following steps,

(a) At given operating conditions, a burst of a small number (e.g., 10 in section 3.1) of pulses is simulated using the complete plasma model until $\Delta n_{e,max} \leqslant 5\%$, with electrical properties calculated during each pulse.
(b) The spatial information about the electron density, electron energy and electric field at the end of the pre-specified burst is stored in a look-up library.
(c) The simulation of subsequent voltage pulses is carried out with the electrical characteristics frozen at the values in the library. The equations for the electric field, electron density and electron energy are switched off.

As a benchmark case, we simulate a burst of 50 nanosecond voltage pulses using both the complete model with the electrical properties calculated in each pulse, and the frozen approach with electrical properties unchanged after the 10th pulse. Figure 6(a) shows the time evolution of the number densities of O, H, and OH at the centre of the discharge gap, predicted by the two models. The simulations are conducted at initial conditions of 144 Torr and 473 K with a pulsing frequency of 40 kHz. The results are shown from the point where the frozen-field calculations begin (10th pulse onwards). It can be inferred that the average O number density remains constant over 50 discharge pulses. The H density, however, increases by more than 100%, from $2 \times 10^{14}\,cm^{-3}$ after 10 pulses to $4.5 \times 10^{14}\,cm^{-3}$ after 50 pulses. The OH number density increases by approximately 30%, from 6×10^{13} to $8 \times 10^{13}\,cm^{-3}$ after 10 and 50 pulses, respectively.

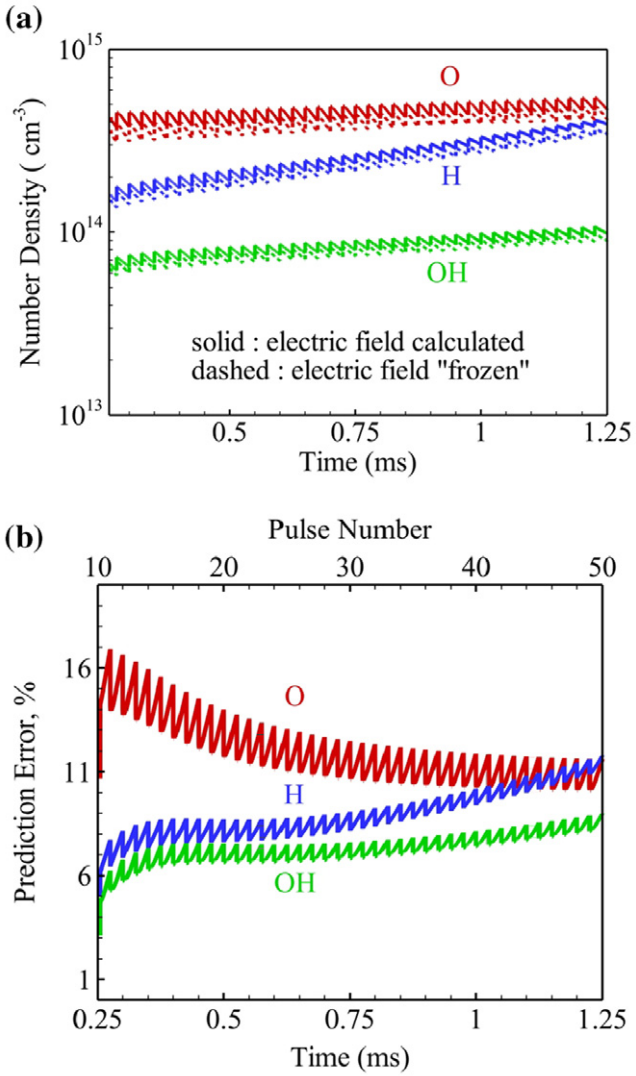

Figure 6. (a) Temporal evolution of O, H, and OH number densities. (b) Prediction error of the frozen model compared to the complete model calculations at the centre of the discharge domain ($P_i = 144$ Torr, $T_i = 473$ K, $\phi = 1$, $f = 40$ kHz).

Figure 6(b) shows the error in the predictions using the frozen-field approach as compared to the complete model calculations at the centre of the discharge volume. The error is defined as the magnitude of the difference in the species density predicted by the frozen and complete models at a particular instant of time, normalized by the latter value. The maximum deviations in the O, H and OH densities are approximately 17%, 12% and 8% respectively. It must be clarified that the error in the predictions varies with the number of pulses. In the case of atomic oxygen density, the performance of the frozen approach improves with increasing pulse number, and the error decreases from 18% after 10 pulses to 12% after 50 pulses. The deviations in the H number density, however, increases with increase in pulse number from 7% after 10 pulses to 12% after 50 pulses. The prediction error in the OH number density increases marginally from 5 to 8% after 10 and 50 pulses respectively. The errors in the electron impact reaction rates calculated using the frozen approach are responsible for

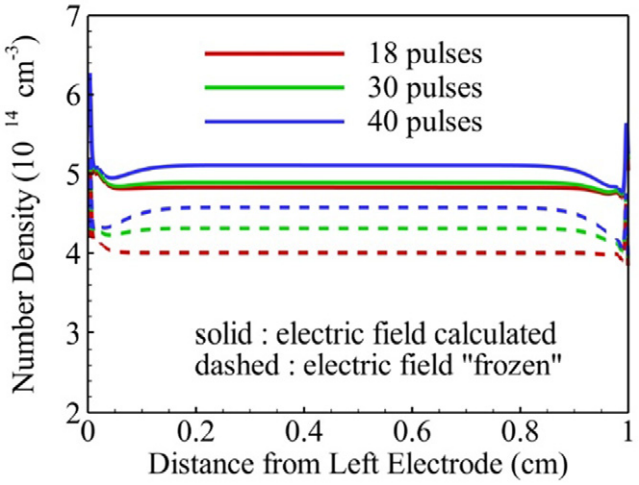

Figure 7. Spatial distribution of O atom number density across the discharge gap predicted by the complete model and with the electric field frozen after 10 pulses ($P_i = 144$ Torr, $T_i = 473$ K, $\phi = 1$, $f = 40$ kHz).

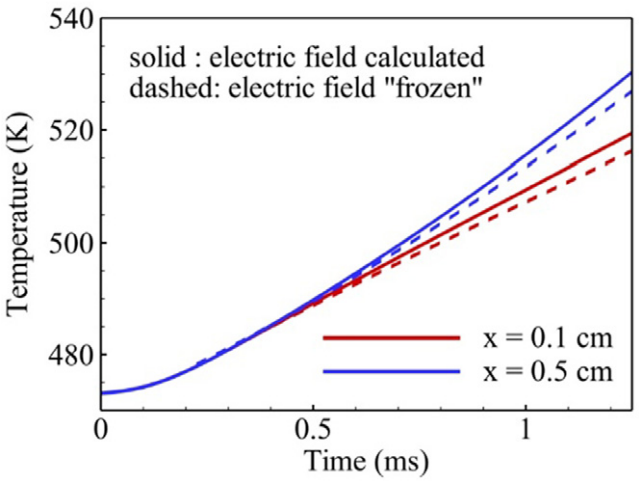

Figure 8. Temporal evolution of temperature at x = 0.1 and 0.5 cm locations ($P_i = 144$ Torr, $T_i = 473$ K, $\phi = 1$, $f = 40$ kHz).

the deviations in the species density evolution in figure 6(*a*). The growth or decay in the species density error shown in figure 6(*b*), is however, dependent on the relative magnitudes of the production and destruction rates of that species. The O atom density is less sensitive to the variation in the electron impact production rate than is the H atom density, hence the frozen approach performs better in predicting the former.

Figure 7 shows the spatial distribution of the atomic oxygen density at the end of the 18th, 30th and 40th pulses. The frozen approach under-predicts the O atom density by approximately 17% throughout the discharge gap, except for the boundary sheath regions, where larger deviations (about 30%) are observed. As noted earlier in figure 6(*b*), the prediction error in the atomic oxygen density decreases with increasing pulse number. After the 40th pulse, the error in the O number density predicted by the frozen approach is less than 10%.

Figure 8 shows the temporal evolution of temperature at two different locations of $x = 0.1$ and 0.5 cm from the left

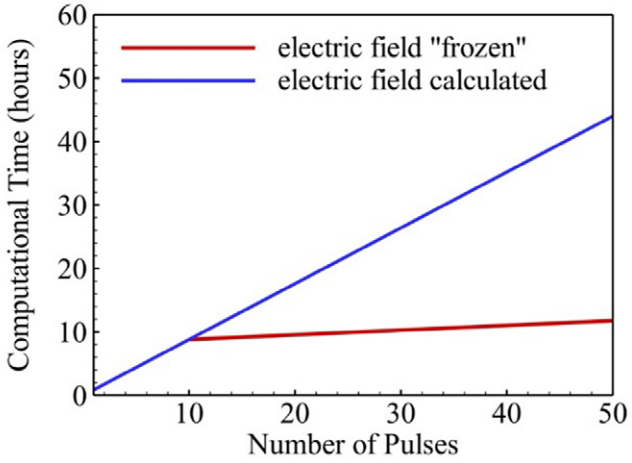

Figure 9. Computational time as a function of number of pulses with the electric field calculated during each pulse compared to the corresponding values with the field frozen after the 10th pulse ($P_i = 114$ Torr $T_i = 473$ K and $f = 40$ kHz).

electrode. Results from the frozen approach agree closely with the detailed plasma model predictions, with less than 5% deviation at both locations. The heat release from quenching of excited species and three-body recombination reactions are responsible for the temperature rise. The small error suggests that the frozen approach is able to accurately predict the rates of quenching and recombination processes in the discharge volume.

The enhancement of computational efficiency of the frozen approach is demonstrated in figure 9 as a function of the number of pulses. The operating conditions are identical to those in figure 6(*a*). The simulations were conducted in parallel over 48 AMD Opteron 2.4 GHz processors connected through Infiniband Fabric switches. The complete model requires approximately 45 h to simulate 50 discharge pulses, where the frozen approach requires only 12 h. A major contributor to this speedup is the use of larger timesteps during each discharge pulse (10^{-9} s when the electric field is frozen as opposed to 10^{-13}–10^{-12} s when the field is calculated). It is worth mentioning that a substantial portion of the computational time for the frozen approach is taken in simulating the first 10 pulses (approximately 1 h per pulse, with the electric field calculated as in the complete model). In contrast, the time to simulate the dynamics of a discharge pulse when the electrical characteristics are frozen is less than 2 min. The savings in computational time increases rapidly with increasing number of pulses. Under the present operating conditions, the ignition of H_2–air mixtures subject to NRPD requires 200–300 voltage pulses (see the next section for details). For such large-scale simulations, the frozen approach is 20 to 30 times faster than the detailed plasma model.

3.3. H_2–air ignition characteristics

The frozen approach described in the previous section substantially improves the computational efficiency of the process. It is thus employed to investigate the effects of pressure and equivalence ratio on NRPD-enhanced ignition of

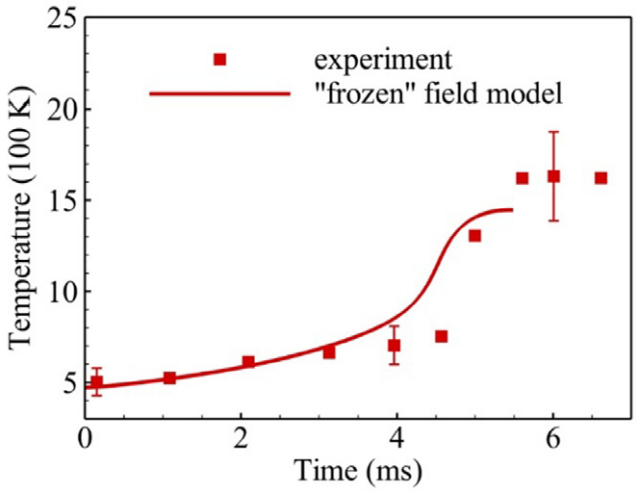

Figure 10. Temperature rise at the centre of the discharge domain predicted by the frozen electric field model compared with measurements from Yin *et al* [17] ($P_i = 114$ Torr, $\phi = 1$, $T_i = 473$ K and $f = 40$ kHz).

H_2–air mixtures. The predicted ignition delay and temperature rise are compared with experimental measurements [17] to validate the frozen modelling approach.

Figure 10 compares the predicted and measured temperature evolution at the centre of the discharge volume at an equivalence ratio of $\phi = 1$. The initial conditions are 104 Torr and 473 K. The pulsing frequency is 40 kHz. The frozen approach provides excellent agreement with experimental data until 3 ms (120 pulses). Beyond this juncture, the temperature is over-predicted by about 20%, resulting in faster ignition compared to measurements. In addition, the model slightly under-predicts the peak temperature after ignition (1500 K as compared to the measured value of 1600 K). The rapid rise in temperature near the ignition point leads to a dramatic reduction in the gas number density, which has a significant impact on the discharge dynamics. The validity of the frozen approach becomes questionable at this juncture, due to the fact that the 'frozen' quantities correspond to the discharge development at lower temperatures. Interestingly, the overall temperature rise predicted by the frozen model deviates less than 20% from the measured data. This phenomenon can be attributed to the partial fuel oxidation triggered by NRPD beyond a threshold temperature of ~700 K [12, 13]. Subsequent application of discharge pulses has a weak effect on the temperature rise because the plasma heating is much smaller than the heat release due to fuel oxidation.

Figure 11(*a*) shows the time evolution of the O, H, OH and HO_2 number densities at the centre of the discharge volume. Atomic oxygen is primarily produced in NRPD by quenching of N_2 by O_2, and through electron impact dissociation of oxygen molecules [22]. H atom is produced with similar kinetic pathways involving H_2 molecules. The following three-body reaction is the primary production pathway for HO_2 and is a major consumption channel of H radicals,

$$H + O_2 + M \rightarrow HO_2. \quad (1)$$

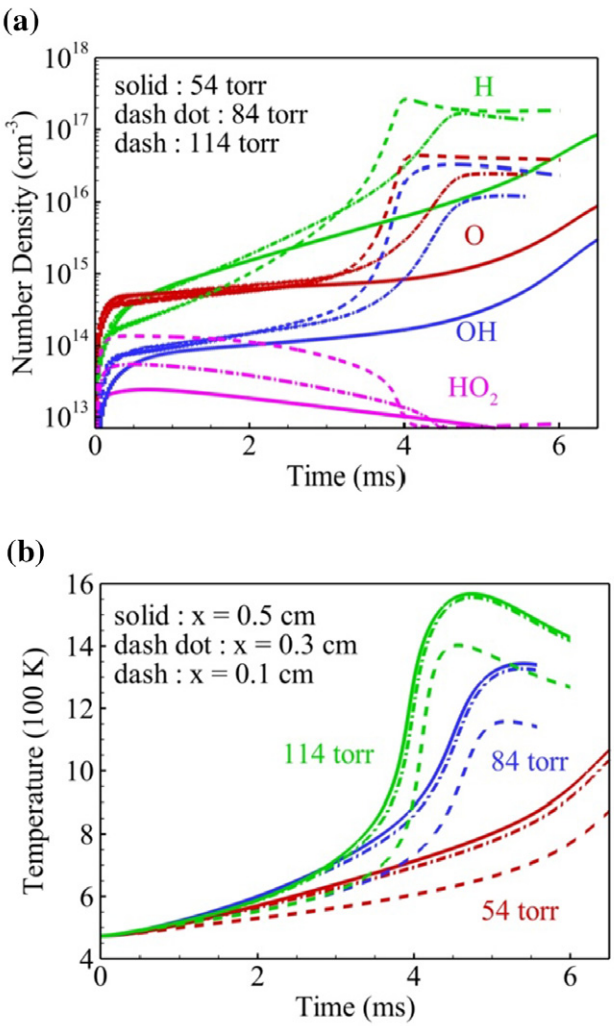

Figure 11. Temporal evolution of (*a*) O, H, OH and HO_2 number densities at the centre of the discharge domain. (*b*) Temperature rise at $x = 0.1$, 0.3 and 0.5 cm locations predicted by the frozen electric-field model for 54 Torr, 84 Torr and 114 Torr pressures, respectively ($T_i = 473$ K, $\phi = 1$ and $f = 40$ kHz).

The rate of the reaction increases with pressure, which explains the accumulation of HO_2 and reduction in the H density with pressure in figure 11(*a*). OH is produced at low temperatures from HO_2 through the following reactions

$$O + HO_2 \rightarrow OH + O_2 \quad (2)$$

$$H + HO_2 \rightarrow OH + OH. \quad (3)$$

The higher HO_2 concentration at 114 Torr results in rapid production of OH from reactions in equations (2) and (3). Figure 11(*b*) shows the time evolution of temperature at three locations ($x = 0.1$, 0.3 and 0.5 cm from the left electrode) for three different pressures of 54, 84, and 114 Torr. The temperature rises linearly with time and is independent of pressure until approximately 1 ms (40 discharge pulses). The higher OH concentrations at 84 and 114 Torr facilitate partial fuel oxidation and heat release from the following reaction,

$$OH + H_2 \rightarrow H + H_2O. \quad (4)$$

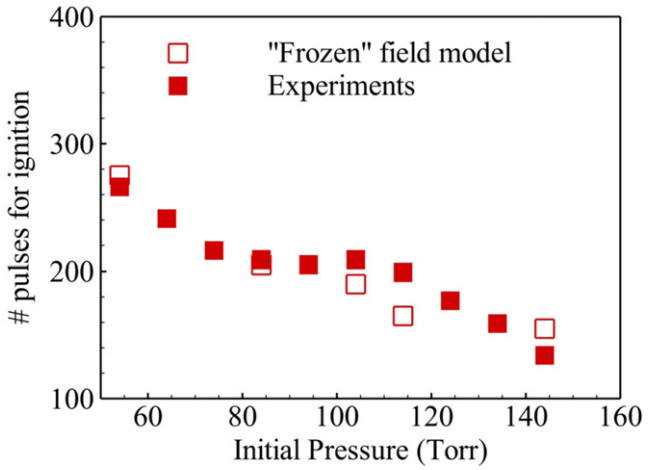

Figure 12. Number of discharge pulses required for ignition as a function of pressure predicted by the frozen electric-field model and measurements from [17] ($T_i = 473$ K, $\phi = 1$ and $f = 40$ kHz).

After 1 ms, the temperature increases in a nonlinear fashion because of heat release from partial fuel oxidation. Finally, the conventional H_2–O_2 chain branching pathways are triggered when the temperature reaches 700 K (at 3 ms for 114 Torr), at which point an exponential increase in temperature takes place, indicative of ignition. Such a temperature profile is typical of ignition of fuel–air mixtures subject to NRPD, as discussed in [13]. Note that the temperature rise at $x = 0.3$ cm closely follows the evolution at $x = 0.5$ cm, suggesting simultaneous, volumetric ignition. A small time delay in the increase in temperature occurs at $x = 0.1$ cm because of the close proximity to the wall, where heat losses are important.

Figure 12 shows the number of discharge pulses required to ignite a stoichiometric ($\phi = 1$) H_2–air mixture subjected to NRPD as a function of pressure. The initial temperature is 473 K, and the pulsing frequency is 40 kHz. Ignition delay time is defined herein as the time for the temperature to rise to 1200 K at the centre of the discharge volume. The ignition delay is reduced by a factor of 2 with increase in pressure from 54 to 144 Torr. This can be attributed to the increase in OH density with pressure, which triggers a low temperature fuel oxidation process through Equation (4) and leads to a rapid temperature rise and ignition, as explained in the previous paragraph. The prediction errors are within 20% of the measurements for all four pressures considered (54, 84, 114 and 144 Torr).

Figure 13(a) shows the temporal evolution of O, H and OH densities at the centre of the discharge domain for $\phi = 0.7$, 1.0 and 1.2. Increase in the equivalence ratio from $\phi = 0.7$ to 1.0 results in a 30% rise in the H_2 density, but only an 8% reduction in the O_2 density. The rates of electron impact dissociation of hydrogen and quenching of excited N_2 states by H_2 molecules show a significant increase with the equivalence ratio. Consequently, the H number density at $\phi = 1.2$ is 1×10^{15} cm^{-3} (at 2 ms, after 80 pulses), almost 40% higher than the value at the same timescale for $\phi = 0.7$ (7×10^{14} cm^{-3}). In contrast, the O and OH number densities are relatively insensitive to the equivalence ratio. Figure 13(b) shows the time evolution of temperature at three locations ($x = 0.1$, 0.3 and 0.5 cm from the left electrode) for different equivalence

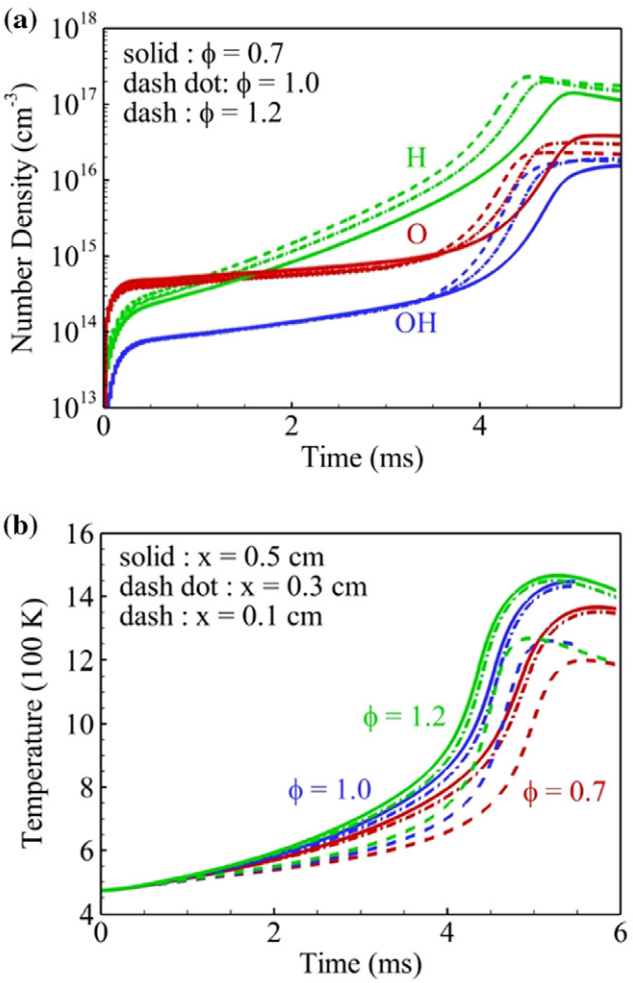

Figure 13. Temporal evolution of (a) O, H, and OH number densities at the centre of the discharge domain, (b) temperature rise at $x = 0.1$, 0.3 and 0.5 cm locations predicted by the frozen electric-field model for equivalence ratios of 0.7, 1.0 and 1.2 respectively. $P_i = 114$ Torr, $T_i = 473$ K and $f = 40$ kHz.

ratios ($\phi = 0.7$, 1.0 and 1.2). The ignition delay time decreases by approximately 20% with increase in the equivalence ratio from 0.7 to 1.2. The ignition delay time at $x = 0.1$ cm is approximately 10% higher than the corresponding value at the centre of the discharge gap, mainly due to heat losses to the walls.

Figure 14 shows the number of pulses required for igniting an H_2–air mixture at initial conditions of 114 Torr and 473 K. Three different equivalence ratios of $\phi = 0.7$, 1.0 and 1.2 are considered. It is found that the ignition delay is a weak function of the equivalence ratio, decreasing from 205 for $\phi = 0.7$ to 195 for $\phi = 1.2$. This is because of the insensitivity of the OH density to variation in the equivalence ratio. In general, the frozen model prediction differs from the measurements by less than 10%. The largest deviation is seen in the case of ignition in rich mixtures (i.e. $\phi = 1.2$).

Good agreement between the ignition measurements and the frozen model predictions over a wide range of operating conditions supports confidence in this technique for efficient simulations of pulsed nanosecond discharges. The proposed approach can be immensely beneficial in performing

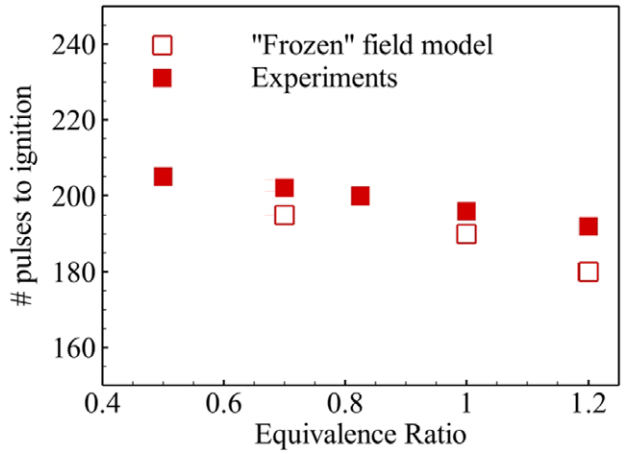

Figure 14. Number of discharge pulses required for ignition as a function of equivalence ratio predicted by the frozen electric-field model and experimental data from [17] ($P_i = 114$ Torr, $T_i = 473$ K and $f = 40$ kHz).

detailed parametric studies and multi-dimensional simulations of pulsed nanosecond discharges.

4. Conclusions

An effective numerical strategy was proposed to expedite simulations of nanosecond repetitively pulsed discharges (NRPDs) without compromise of solution accuracy. The 'frozen electric-field' modelling approach was based on the periodic nature of NRPD, wherein the electrical characteristics reached a stationary state after a few voltage pulses. The spatial distributions and temporal evolution of the electric field, electron density and electron energy were stored in a look-up library. The subsequent pulses were simulated by freezing the electrical properties to the values in the library. This allowed for the timestep size to be increased by four orders of magnitude from 10^{-13} to 10^{-9} s. It was found that the frozen model was five times faster than the complete model in simulating 50 pulses, and showed a speedup of up to 30 times for large-scale simulations (200–300 pulses). The simulation results compared favourably with the complete plasma model predictions, and showed good agreement with the ignition delay and temperature measurements of H_2–air mixtures subject to pulsed nanosecond dielectric barrier discharges at different pressures (54–144 Torr), and equivalence ratios (0.7–1.2). The ignition delay reduced by a factor of 2 with increase in pressure from 54 to 144 Torr. This was attributed to the increase in the OH density with pressure, which triggered low-temperature fuel oxidation and led to rapid temperature rise and ignition. In contrast, the increase in the H_2–air equivalence ratio from 0.7 to 1.2 marginally decreased the ignition delay by about 20%. Such behaviour resulted from the insensitivity of OH production rates to the variation in the equivalence ratio.

Acknowledgments

This work was supported by MURI research grant FA9550-09-0602 from the Air Force Office of Scientific Research, with Dr Chiping Li as technical monitor.

References

[1] Starikovskiy A and Aleksandrov N 2013 Plasma-assisted ignition and combustion *Prog. Energy Combust. Sci.* **39** 61–110
[2] Pilla G, Galley D, Lacoste D A, Lacas F, Veynante D and Laux C 2006 Stabilization of a turbulent premixed flame using a nanosecond repetitively pulsed plasma *IEEE Trans. Plasma Sci.* **4** 2471–77
[3] Leonov S B, Yarantsev D A, Napartovich A P and Kochetov I V 2006 Plasma-assisted combustion of gaseous fuel in supersonic duct *IEEE Trans. Plasma Sci.* **34** 2514–25
[4] Dutta A, Yin Z and Adamovich I V 2011 Cavity ignition and flameholding of ethylene–air and hydrogen–air flows by a repetitively pulsed nanosecond discharge *Combust. Flame* **158** 1564–76
[5] Unfer T and Boeuf J P 2009 Modelling of a nanosecond surface discharge actuator *J. Phys. D: Appl. Phys.* **42** 194017
[6] Poggie J, Adamovich I V, Bisek N and Nishihara M 2013 numerical simulation of nanosecond pulse electrical discharges *Plasma Sources Sci. Technol.* **22** 015001
[7] Adamovich I, Choi I, Jiang N, Kim J, Keshav S, Lempert W, Mintusov E, Nishihara M, Samimy M and Uddi M 2009 Plasma assisted ignition and high-speed flow control: non-thermal and thermal effects *Plasma Sources Sci. Technol.* **18** 034018
[8] Laroussi M, Hynes W, Akan T, Lu X and Tendero C 2008 The plasma pencil: a source of hypersonic cold plasma bullets for biomedical applications *IEEE Trans. Plasma Sci.* **36** 1298–9
[9] Shi J, Zhong F, Zhang J, Liu D and Kong M G 2008 A hypersonic plasma bullet train traveling in an atmospheric dielectric-barrier discharge jet *Phys. Plasmas* **15** 013504
[10] Ayan H, Staack D, Fridman G, Gutsol A, Mukhin Y, Starikovskii A, Fridman A and Friedman G 2009 Application of nanosecond-pulsed dielectric barrier discharge for biomedical treatment of topographically non-uniform surfaces *J. Phys. D: Appl. Phys.* **42** 125202
[11] Breden D, Miki K and Raja L 2011 Computational study of cold atmospheric nanosecond pulsed helium plasma jet in air *Appl. Phys. Lett.* **99** 111501
[12] Nagaraja S, Adamovich I and Yang V 2013 Multi-scale modeling of pulsed nanosecond dielectric barrier discharges in plane-to-plane geometry *J. Phys. D: Appl. Phys.* **46** 155205
[13] Nagaraja S, Yang V, Yin Z and Adamovich I 2014 Ignition of hydrogen–air mixtures using pulsed nanosecond dielectric barrier plasma discharges in plane-to-plane geometry *Combust. Flame* **161** 1026–37
[14] Tholin F and Bourdon A 2013 Simulation of the stable 'quasi-periodic' glow regime of a nanosecond repetitively pulsed discharge in air at atmospheric pressure *Plasma Sources Sci. Technol.* **22** 045014
[15] Starikovskiy A, Shneider M, Marinov D and Starikovskaia S 2014 Thermal ionization instability development in air plasma generated by repetitive NS dielectric barrier plasma *AIAA 52nd Aerospace Sciences Meeting (National Harbour, MD)*
[16] Yin Z, Montello A, Carter C, Lempert W and Adamovich I 2013 Measurements of temperature and hydroxyl radical generation/decay in lean fuel–air mixtures excited by a repetitively pulsed nanosecond discharge *Combust. Flame* **160** 1594–1608
[17] Yin Z, Takashima K and Adamovich I V 2011 Ignition time measurements in repetitive nanosecond pulse hydrogen–air plasmas at elevated initial temperatures *IEEE Trans. Plasma Sci.* **39** 3269–82

[18] Hagelaar G and Pitchford L 2005 Solving the Boltzmann equation to obtain electron transport coefficients and rate coefficients for fluid models *Plasma Sources Sci. Technol.* **14** 722

[19] Konnov A 2008 Remaining uncertainties in the kinetic mechanism of hydrogen combustion *Combust. Flame* **152** 507–28

[20] Popov N 2011 Fast gas heating in a nitrogen–oxygen discharge plasma: Part I. Kinetic mechanism. *J. Phys. D: Appl. Phys.* **44** 285201

[21] Takashima K, Yin Z and Adamovich I V 2013. Measurements and kinetic modeling of energy coupling in volume and surface nanosecond pulse discharges *Plasma Sources Sci. Technol.* **22** 015013

[22] Stancu G D, Kaddouri F, Lacoste D and Laux C 2010 Atmospheric pressure plasma diagnostics by OES, CRDS and TALIF *J. Phys. D: Appl. Phys.* **43** 124002